Light-Harvesting Battery Charger for IoT Sensor Node

Maísa Seidi

***Abstract*—This article describes the design of a light-harvesting battery charger that uses the energy captured by a photovoltaic (PV) cell to charge a 1.2 V nominal voltage NiMH battery, to be used in an IoT sensor node. The whole system is developed to be fabricated in a 65nm CMOS proccess. A simulation-ready equivalent model of the battery is developed based on experimental procedures. The design and implementation of the system is presented and tested in simulation. Battery management with overcharge and overdischarge protection for the battery are incorporated. Finally, a full system layout with a silicon footprint of 0.04 mm^2 is proposed and validated in simulation with the source and battery models developed, for different operation conditions, temperatures, and process corners.**

***Index Terms*—Battery charger; Light harvesting; Battery electrical model; Internet of Things; CMOS technology; Solar cells.**

I. Introduction

THE rapid development of the Internet of Things brings a high demand for more autonomous and self-powered miniaturized devices. These electronic devices are typically powered by small batteries, but the limited battery lifetime imposes a limitation on the durability of their operation. Energy harvesting presents itself as an efficient way to power and recharge these devices, by alleviating the cost and difficulty of wiring a large number of these objects, thus providing a practical solution for more autonomous IoT nodes, that can become less dependent on external power sources. Several energy harvesting sources can be used for this purpose, such as light, motion, heat, vibration and others. Out of the above, light harvesting is typically the most consolidated option due to its abundance and higher power density in comparison with the referred alternative sources. Notwithstanding, there are some limitations to light-harvested energy. For starters, the energy is intermittent, as sunlight is not always available, indoor light can be a poor substitute and additionally, small PV cells capture only a small fraction of the available light. As such, these light-harvesting systems are not sufficient to feed the devices on their own; a storage device, such as a battery, should be used to store the energy for a continuous and reliable operation of these electronic circuits. The V6HR type micro-battery is considered for that end, due to its relatively high capacity and small size. An experimental procedure is carried on to develop an equivalent model for this battery. The selected source to supply the battery is the ONP1.2-12x24 flexible solar cell. A harvester system is developed, which receives energy from the PV cell, and constantly monitors the energy available in the environment and the battery's state of charge, to decide when the system should be switched on to charge the battery, and when the battery is in the right conditions to feed the final load. Figure 1 presents a top illustration of the system and its connections to the PV cell, the battery and the final load. The purpose of this work is to design the fully integrated system enclosed in the blue box on the figure.

Manuscript received April 19, 2021; revised August 16, 2021.

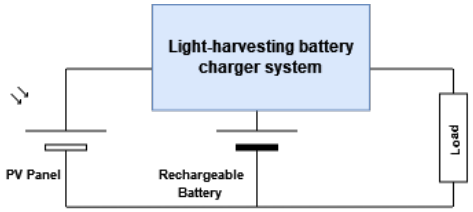

Fig. 1. Illustration of the top system to be designed.

In the following section the methodology adopted for the development of the source and battery models is described. Afterwards, the system design is presented with a brief description of the different circuits that composes the harvester. Lastly, simulation results for different operation conditions are presented and discussed along with the final conclusion of this study.

II. Battery and source modeling

A. Battery model

Several electrical equivalent models for batteries have been proposed by different authors. For the purpose of this work, the electrical circuit model proposed in [1] is considered, which is presented in figure 2. This model prevails by providing a very good approximation of the electrical characteristics that represents the battery's operation, accurately reflecting the battery's run time, as well as its stationary and transient responses.

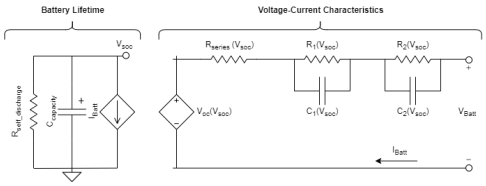

Fig. 2. Electrical model considered for the battery.

The presented model can be subdivided into two distinct branches: one that simulates the battery's lifetime and another that represents its transient response and the V-I characteristic.

The first branch on the left is constituted by a self-discharge resistor that reflects the energy losses that occurs when the

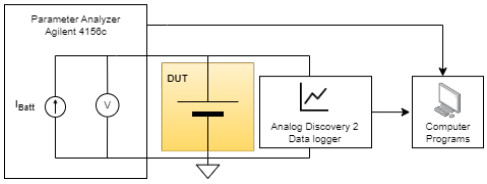

Fig. 3. Battery test system.

battery is not being used for a long period of time, due to the chemical processes inherent to its constitution. In parallel with this resistance, there is a capacitor that represents the full capacity or energy stored in the battery, at a given moment. This capacitor's value is defined as in equation 1.

$$C_{capacity} = 3600 \times C_{nom} \times f_1(Cycle) \times f_2(Temp)\ [C] \quad (1)$$

where C_{nom} is the nominal capacity in Ah and f1(Cycle) and f2(Temp) represent the battery's charge variation with the number of cycles (defined as the number of charge and discharge cycles) and with the temperature, respectively. For the purpose of this work, the parameters' dependence with the number of cycles and temperature are ignored, since they have negligible effects, and because including them would significantly increase the complexity of the test system.

The voltage V_{SOC} quantitatively represents the *State of Charge* (SOC) of the battery, taking values between 0 (battery fully discharged) and 1 (battery fully charged). The dependent current source serves to charge or discharge the capacitor, dynamically changing the voltage V_{SOC}, thus modeling the relationship between the state of charge of the battery and its current.

The branch on the right represents the V-I characteristic of the battery. The dependent voltage source describes the non-linear relationship between the open circuit voltage and the battery's state of charge. The series resistance represents the internal resistance of the battery and the RC branches simulate the relaxation effects, with one branch representing the short time constant and the other branch the long time constant of the battery. All the parameters in the model are multi-variable functions of the *State of charge*, current, temperature, and cycle number.

1) Experimental Procedure: In order to estimate the values of the model's parameters, an experimental procedure is necessary to collect adequate data for their computation. Figure 3 illustrates the test system set up for the experiment.

References [2], [3] and [4] all present different methods to obtain an equivalent model for the battery. After thoroughly studying and considering all these methods, a suitable procedure was developed for this work.

The carried out test consisted on applying charging and discharging cycles to the battery and subsequently observing its terminal voltage variation. A current-controlled charge/discharge method was used, with the aid of the *Agilent 4156c Parameter Analyzer*. A test system was programmed in the equipment so that current pulses were applied to the battery to either charge or discharge it, in a periodic manner, while measuring the terminal voltage of the battery. Since the experimental tests take a considerable amount of time, the *Analog Discovery 2* board was simultaneously used as a data logger to continuously measure and store the battery's terminal voltage.

Initially, a 16-hour charge was carried out, with a current of 0.1C (0.620 mA), according to the manufacturer's instructions, to ensure that the battery was fully charged with a SOC of 100%. After charging, a rest time is required for the battery to reach equilibrium, and for the open circuit voltage to be measured, so a waiting time of one hour was established.

With the battery fully charged, a discharge with current pulses was then carried out. The purpose of using this type of charge/discharge is to analyze, for different battery charge states, its transient behavior, in order to obtain the parameters of the equivalent model, since these vary with the battery's state of charge. Pulses of 1C (6.2 mA - rated current) with a duration of 10 minutes and intervals of 10 minutes between each pulse were selected, considering that to be a sufficient time for voltage stabilization. The purpose of this test is to discharge the battery from 100% to 0% and observe the evolution of the voltage in the interval between pulses. This way, it is possible to obtain the parameter values and the open circuit voltage of the battery for each value of the state of charge. After the discharge test, the same procedure was applied to charge the battery with current pulses of 10 minutes, with the nominal value, followed by intervals of 10 minutes, until the battery was 100% charged. It should be noted that the time required for the battery to fully reach the steady state is approximately 5 hours. However, this delay leads to extensive tests, requiring several days for a charge or discharge cycle to be completed. For this reason, a shorter interval of 10 minutes was chosen.

2) Model extraction: As previously mentioned, the parameters of the equivalent model are not static, varying with the SOC, current, temperature and cycle number of the battery. For simplicity, only the SOC variation is accounted for in this model. The results obtained experimentally allow for the estimation of these parameters for different points of the SOC, through the analysis of the battery's voltage after the application of each charge/discharge pulse. The method used here is based mainly on the one presented in [5].

Figure 4 presents a close up of one area of the pulse-discharge graph, where the evolution of the voltage at the battery's terminals resulting from the application of the pulse discharge can be observed in more detail. This figure shows the time frame used to compute the battery's parameters, following the procedure described below.

Analyzing the figure, a linear decrease in the voltage value is observed during the first 10 minutes, caused by the constant current discharge. When the pulse is interrupted, the sudden increase in the voltage is due to the absence of current in the resistor R_{series}, which allows to obtain its value through

$$R_{series} = \frac{V_2 - V_1}{I} \quad (2)$$

where I is the discharge current and V_1 and V_2 are the

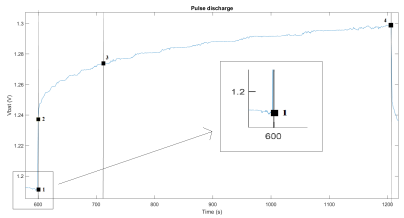

Fig. 4. Time frames used in the computation of the equivalent circuit's parameters.

voltages at points 1 and 2, respectively. The remaining parameters are estimated by fitting the transient response curve of the relaxation zone with an exponential function. The voltage between points 2 and 3 can be described by the following exponential function

$$V_{bat} = a_0 + a_1 e^{-\frac{t}{\tau_1}} + a_2 e^{-\frac{t}{\tau_2}} \tag{3}$$

where the time constants correspond to

$$\tau_1 = R_1 C_1 \ and \ \tau_2 = R_2 C_2 \tag{4}$$

Using a computational calculation software, the experimentally acquired data was processed and the relaxation curves were individually adjusted with exponential functions, according to the windows defined in figure 4. Tables I and II present the results obtained for the model parameters, for the different stages of the SOC during both discharge and charge, respectively.

TABLE I
EXTRACTED PARAMETERS FOR DISCHARGE EQUIVALENT MODEL

SOC (%)	**Rseries (Ω)**	**R1 (Ω)**	**C1 (F)**	**R2 (Ω)**	**C2 (F)**
100.0	7.58	9.91	0.099	7.42	28.85
83.3	8.71	6.80	0.151	7.30	26.71
66.7	7.42	3.31	6.919	7.87	39.57
50.0	9.84	9.88	0.094	9.15	21.10
33.3	11.94	6.39	0.707	10.05	24.64
16.7	25.02	7.56	0.007	12.95	14.46
0.0	115.00	414.03	0.022	95.23	0.69

TABLE II
EXTRACTED PARAMETERS FOR CHARGE EQUIVALENT MODEL

SOC (%)	**Rseries (Ω)**	**R1 (Ω)**	**C1 (F)**	**R2 (Ω)**	**C2 (F)**
0.0	9.84	11.83	0.157	9.07	23.98
14.3	7.74	9.98	0.091	7.66	27.61
28.6	8.06	6.30	0.282	7.21	28.52
42.9	8.06	9.71	0.173	8.45	22.35
57.1	7.42	8.11	0.007	11.91	15.19
71.4	8.23	7.24	0.007	16.65	13.49
85.7	9.35	5.37	2.907	17.77	20.22
100.0	9.84	4.99	4.496	16.37	22.06

Figures 5 and 6 present V_{OC}'s variation with V_{SOC} for both charge and discharge, respectively. To illustrate this relationship, the SOC in percentage was already converted into a voltage between 0 V and 1 V. A 7th order polynomial was fitted to the above mentioned curves, as described in 5, to derive the open circuit voltage's dependence with the state of charge.

$$V_{OC} = p_1 V_{SOC}^7 + p_2 V_{SOC}^6 + p_3 V_{SOC}^5 + p_4 V_{SOC}^4 + p_5 V_{SOC}^3 + p_6 V_{SOC}^2 + p_7 V_{SOC} + p_8 \tag{5}$$

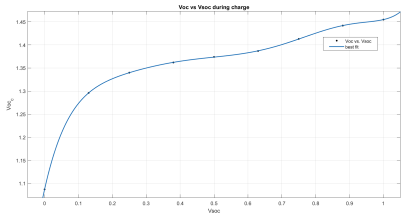

Fig. 5. V_{OC}'s variation with V_{SOC} during charge

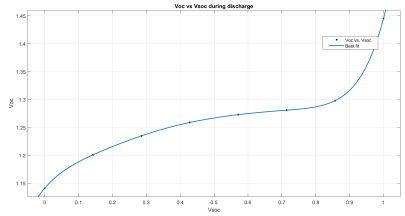

Fig. 6. V_{OC}'s variation with V_{SOC} during discharge

The coefficients obtained for each of the two models with 95% confidence bounds and an R-square of 1 are presented in table III.

TABLE III
COEFFICIENTS FOR THE POLYNOMIAL DESCRIBING V_{OC}'S VARIATION WITH V_{SOC} FOR CHARGE AND DISCHARGE

Coefficients	**Charge**	**Discharge**
p_1	31.44	16.5
p_2	-121.6	-51.63
p_3	190.2	66.29
p_4	-156	-44.65
p_5	73.12	16.84
p_6	-20.16	-3.771
p_7	3.285	0.7205
p_8	1.087	1.141

3) Model simulation: The extracted model was implemented in Cadence Virtuoso and an analogous simulation to the experimental procedure was carried out, to assess the model's behaviour and its accuracy in comparison to the laboratory results. The general model of the battery is presented in figure 7.

To simplify the models, the parameters' variation with the SOC were not accounted for in this implementation, so static values were adopted for each of the components. Average values were initially selected and continually fine-tuned based on the simulation results. The final selected values for the models' parameters are presented in table IV.

A transient analysis was carried out, with the current source acting as a mean to pulse-charge and pulse-discharge the

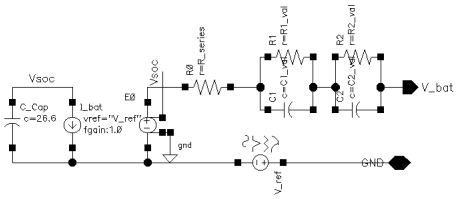

Fig. 7. Equivalent model of the battery implemented in Virtuoso.

TABLE IV
FINAL PARAMETERS USED IN THE EQUIVALENT CIRCUIT MODELS.

	R_series (Ω)	**\R1 (Ω)**	**C1 (F)**	**R2 (Ω)**	**C2 (F)**
Charge	8	8	20	8	0.1
Discharge	8	8	0.1	8	20

battery, depending on the value's polarity. An initial condition is specified to define the battery's initial SOC as 0 and 1 for the charge and discharge simulation, respectively. Figures 8 and 9 present the battery's terminal voltage for each of the two simulation conditions.

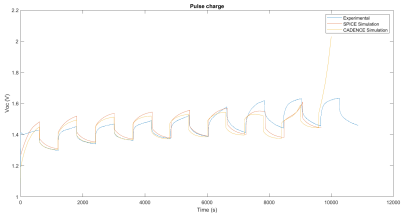

Fig. 8. Terminal voltage during charge process: experimental vs simulation results.

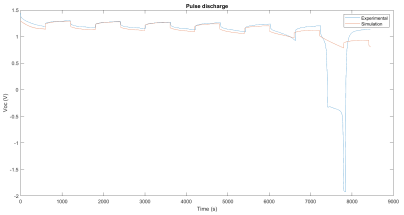

Fig. 9. Terminal voltage during discharge process: experimental vs simulation results.

As demonstrated, the models are able to replicate the terminal voltage's behavior of the battery during the charge and discharge cycles, presenting a similar characteristic to the experimental results. The discrepancies observed are due mainly to the discontinuity of the experimental equipment in the application of the current pulses. The parameter analyzer takes approximately one second to switch the current from zero to the specified value and this delay is not constant, making it burdensome to replicate the exact same behaviour in simulation. Furthermore, the disparity in the voltage values can be explained by the theoretical approximations made in the model extraction, namely the parameter's dependence on temperature and cycle number, but most importantly, by the impossibility of replicating the parameter's variability with the battery's SOC.

In the experimental results, it is noticeable that the battery is discharged into reverse in the last current pulse application. Efforts were made with different test configurations applied to different batteries, but preventing this behaviour posed a challenge due to the available lab equipment's limitation of measuring the battery's SOC. This behaviour however is not replicated in the model because it is resultant from the battery's internal chemical functioning and cannot be fully described using the electrical equivalent model.

B. PV Cells model

For the purpose of this work, the *one diode five-parameter model* circuit model, presented in figure 10, is adopted to represent the PV solar cells.

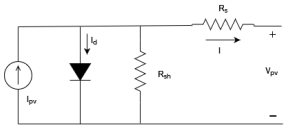

Fig. 10. Equivalent circuit for a photovoltaic cell.

In the model, the ideal current source represents the current delivered by the solar cell in accordance with the incident radiation. In parallel with the source, there is an ideal diode that represents the cell p-n junction. In open-circuit a voltage V_{oc} appears at the PV cell's terminals. Two additional resistors are included, R_{sh} and R_s, to account for the electrical losses of the cell. The PV cell's current can be described by the following expression 6.

$$I = I_{pv} - I_0 \left[\exp\left(\frac{V_{pv} + IR_s}{aV_T} \right) - 1 \right] - \frac{V_{pv} + IR_s}{R_{sh}} \quad (6)$$

where I_0 is the reverse saturation current of the diode, a is the ideality factor of the diode and V_T is the thermal voltage as described in 7

$$V_T = n\frac{kT}{q} \quad (7)$$

The thermal voltage V_T depends, in turn, on the number of cells in series n, on the Boltzman constant k, on the temperature T and on the electron charge q.

To sum up, in order to build a simulation-ready model of the PV cell, the following five parameters of the model must be obtained: R_{sh}, R_s, I_0, I_{pv} and a. The procedure carried out is described in the following sub-section.

1) Model extraction: The model's parameters can be computed based on the I-V characteristic of the PV cell, which is presented in figure 11. Using an extraction tool, this data was acquired from the datasheet and introduced in MATLAB.

The parameters of the equivalent model are not static, varying with the light intensity and with the wavelength of the incident radiation. For simplicity, the computation of these parameters is done considering the PV cells under full sun, which corresponds to an irradiance of 1000 W/m^2 (filled curve on figure 11).

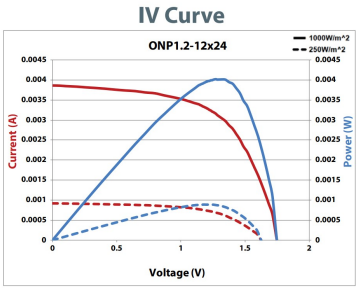

Fig. 11. I-V Characteristic of PV cell from datasheet.

Adopting the method presented in [6], the following expressions are considered to compute the five parameters of the model.

$$\frac{1}{(V_{mp}-I_{mp}R_s)-aV_T(V_{mp}I_{sc}-V_{oc}I_{mp})}\times \frac{aV_TV_{mp}(2I_{mp}-I_{sc})}{(V_{mp}I_{sc}+V_{oc}(I_{mp}-I_{sc}))}=\exp\left(\frac{V_{mp}+I_{mp}R_s-V_{oc}}{aV_T}\right) \tag{8}$$

$$R_{sh}=\frac{(V_{mp}-I_{mp}R_s)(V_{mp}-R_s(I_{sc}-I_{mp})-aV_T)}{(V_{mp}-I_{mp}R_s)(I_{sc}-I_{mp})-aV_TI_{mp}} \tag{9}$$

$$I_0=\frac{(R_{sh}+R_s)I_{sc}-V_{oc}}{R_{sh}exp(\frac{V_{oc}}{aV_T})} \tag{10}$$

$$I_{pv}=\frac{R_{sh}+R_s}{R_{sh}}I_{sc} \tag{11}$$

By performing an initial estimate of the ideality factor a, it is possible to reduce the number of unknown variables from five to four, which makes the above expressions sufficient in determining the remaining parameters of the model. The ideality factor's value is normally bound to a small interval, typically between 1 and 1.5, for a single junction solar cell [6]. Selecting an initial value of 1.5 for parameter a, the results obtained for the model are shown in table V.

TABLE V
FIVE-PARAMETERS OBTAINED FOR THE PV CELL'S MODEL

a	R_{sh} (Ω)	R_s (Ω)	I_0 (mA)	I_{pv} (mA)
1.5	1958	152	0	4

2) Model Simulation: With the results obtained analytically, a simulation-ready model of the PV cell was implemented in Virtuoso, as presented in figure 12.

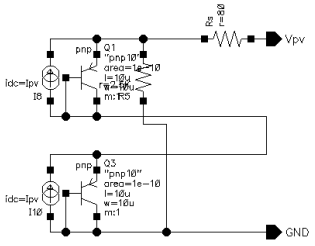

Fig. 12. PV panel's model implemented in Virtuoso: schematic and symbol.

The model implemented represents two cells in series, which together compose the device used in this project. A diode-connected PNP bipolar transistor is used to represent the model's diode. Using the estimate values from table V as a starting point, the model's parameters were continually fine-tuned to match the manufacturer's data. Figure 13 shows the I-V curve of the final model obtained, against the experimental V-I characteristic.

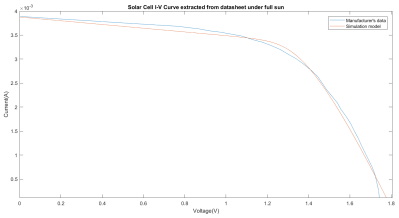

Fig. 13. I-V Characteristic of the developed model vs the datasheet data.

III. System Architecture

The energy harvester's system primary target is to perform battery charging and battery management. For this system, the battery charging is performed through the direct charging method, in which the PV cells are directly connected to the battery through a switch. An alternative for this fully CMOS solution would be to include *switched-capacitors* or inductive DC-DC converters with MPPT tracking, which ensures that the PV cells are always working at maximum power point. However, these circuits would require a larger die-area to accommodate for the large sizes of the capacitors/inductors, and would require a higher operating frequency, which would greatly increase the power consumption of the system. Furthermore, the direct charging method can achieve even higher efficiency than other implementations that use DC-DC converters [7]. To increase the efficiency, it is advisable that the PV cells operate as close as possible to the maximum power point, and since in direct charging V_{pv} always follows V_{bat}, this can be ensured by choosing a PV module with a V_{MPP} close to the V_{EOC} of the battery. Considering that the V_{MPP} does not change significantly with the lighting conditions, the operation at MPP is secured throughout most of the charge and discharge process, the highest deviation corresponding to the situation where the battery is discharged and V_{bat} drops to 1 V.

Figure 14 presents the proposed system's architecture, detailing the different functional blocks that compose the circuit.

The system is composed of two switches, which allows to open/close the connection between the solar cells, the battery, and the final load, the comparator circuits, which are used to monitor and compare the different voltage levels existent in the system, and a decision circuit which controls the charge/discharge process. A regular comparison is performed between the PV cells' and the battery's terminal voltages to assess when the charging process should take place. The switch S1 is controlled by the output of Comparator 1 and is only enabled when the PV cells' terminal voltage is higher than the battery's terminal voltage. When the PV cells' voltage

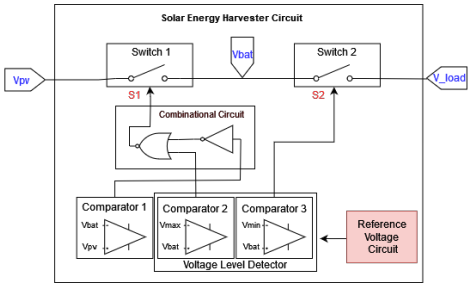

Fig. 14. Solar Harvester functional blocks.

is lower than the battery's voltage, the switch is turned off to ensure that the battery is not discharged through the PV cells. The implemented battery management process consists on the verification that the battery remains within the specified V_{min} and V_{max} voltages during charge and discharge, to prevent overcharge and deep-discharge, which reduces battery lifetime and its overall performance. This is accomplished by a Voltage Level Detector Circuit that continually compares the battery's terminal voltage with the defined *End of Charge* (EOC) and *End of Disharge* (EOD) voltage levels, and decides whether the charge/discharge should be interrupted. According to the datasheet, the V_{EOC} and V_{EOD} voltages for this battery is approximately 1.5 V and 0.9 V, respectively. For the purpose of this work, the minimum battery voltage for the system's operation will be assumed as 1 V, so the defined limits for the system will be V_{min} = 1 V and V_{max} = 1.5 V. At last, a simple logic combinational circuit is used to manage the system, appropriately verifying all the aforementioned conditions and controlling the selection of the switches state.

The system's schematic implemented in Virtuoso is presented in figure 15.

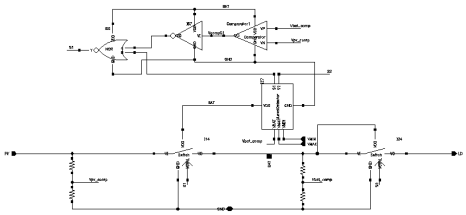

Fig. 15. System's schematic.

A. Comparator

Considering the low speed operation necessity of the solar harvester, a simple two-stage self-biased Operational Amplifier is used as a Comparator, in an open-loop configuration. The implemented circuit is presented in figure 16.

This topology uses an NMOS differential pair with a cascode current mirror that improves the output resistance of the OpAmp. Two high resistance polysilicon resistors in series are used for biasing, as a means to optimize layout space. The comparator was designed with a push-pull output configuration and the current in the first branch is approximately 20 μA. A simple latch is included at the output to improve the quality of the signal for digital control.

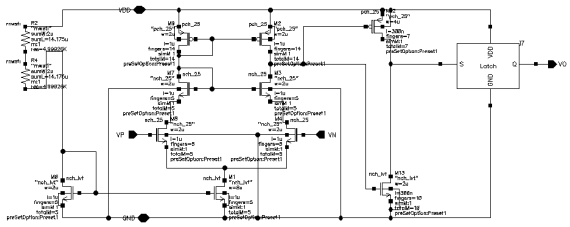

Fig. 16. Comparator schematic.

B. Voltage Level Detector

The Voltage Level Detector circuit compares the battery's voltage with V_{EOC} and V_{EOD} threshold voltages to oversee that V_{bat} does not go beyond these values. The threshold voltages are generated by a BGR (external to the system) and these voltages are each compared with V_{bat} through the use of two individual Comparators. The schematic of this block is presented in figure 17.

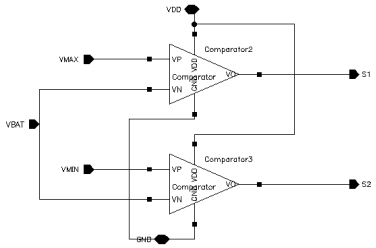

Fig. 17. Voltage Level Detector schematic.

The battery's datasheet specifies the V_{EOC} and V_{EOD} voltages as approximately 1.5 V and 0.9 V, respectively. For the purpose of this work, we will consider the minimum battery voltage for the system operation as 1 V. Considering that the whole system will be supplied by the NiMH battery, the supply voltage becomes a limitation in the design of the BGR, due to the inability to generate reference voltages that are higher than the supply voltage. For this matter, the reference voltages selected to be generated were 0.75 V and 0.5 V to represent both V_{EOC} and V_{EOD} , respectively. By using a voltage divider with resistors in series, an accurate comparison is achieved between the battery's terminal voltage and the threshold voltages.

C. Combinational Circuit

The control unit of this circuit essentially consists on the management of the two switches, which can be either ON or OFF, depending on the set of conditions specified for each case.

As previously mentioned, S1 must be ON only if the following two conditions are met: if the solar cell's terminal voltage is higher than the battery's voltage, so that there is no discharge through the cell, and while the battery's voltage is less than the EOC terminal voltage. As for S2, which controls the battery's charge of the load, it should be ON only if the battery's voltage is higher than the specified EOD voltage of 1

V. Due to the simplicity of the system, a simple combinational circuit is used to verify these statements, based on the truth-table presented in Table VI. The signals C1, C2 and C3 correspond respectively to the output of the first, second and third comparators, specified on figure 14.

TABLE VI
TRUTH-TABLE FOR THE COMBINATIONAL CIRCUIT

C1	C2	C3	S1	S2
0	0	0	0	0
0	0	1	0	1
0	1	0	0	0
0	1	1	0	1
1	0	0	1	0
1	0	1	1	1
1	1	0	0	0
1	1	1	0	1

From the above table, the following logic relations can be obtained:

$$S1 = C1 \cdot \overline{C2} \tag{12}$$

$$S2 = C3$$

By applying boolean algebra to 12, the combinational logic for S1 can be further simplified to

$$S1 = \overline{\overline{C1} \oplus C2} \tag{13}$$

which corresponds to the final circuit used in the system. Figure 18 presents the gates used to control S1.

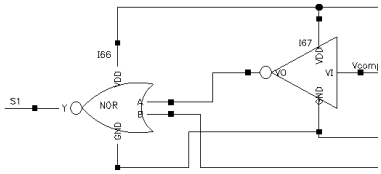

Fig. 18. Logic gates used to control S1.

D. Switches

In this system, the switches are used to control when the PV cells are connected to charge the battery and when the battery is connected to feed the load. Since a direct charging method is employed, the switch should be large enough so that the voltage drop between Vpv and Vbat is negligible. When the switch is turned ON, Vpv will follow Vbat and charge the battery.

For this purpose, a transmission gate is used for the switch, as presented in figure 19.

The transmission gate consists of one NMOS transistor in parallel with a PMOS transistor. The principle of this circuit is to bias the transistors with complementary control signals to ensure that they are both either on or off simultaneously. When the control signal is high, both transistors will be on and the switch will be closed; when the control signal is low, both transistors will be off and the switch will be open with

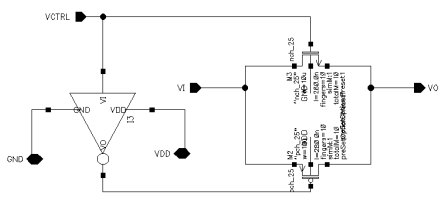

Fig. 19. Switch schematic.

no current flowing through it, ideally. The on resistance value of the switch is shown in 14.

$$R_{on} = \frac{V_{on}}{I_{on}} \approx 59\,\Omega \tag{14}$$

E. System layout

After designing and testing the circuits all together, the full layout of the system was developed, as presented in figure 20. The final layout resulted in an area of 0.1 x 0.043 mm^2. Table VII presents in detail the die area occupied by each of the common blocks that compose the system.

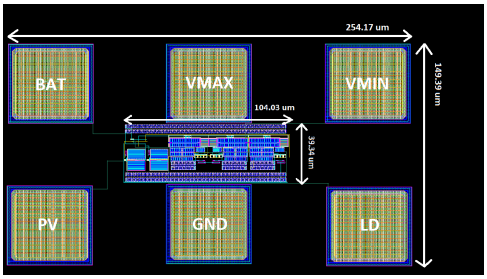

Fig. 20. System layout.

TABLE VII
DIE AREA OF FUNCTIONAL BLOCKS AND COMPONENTS

Functional Block	**Die Area** $(\mu m)^2$
Inverter	4.18
NOR gate	7.25
Switch	192.79
Comparator	617.50
Voltage Level Detector	1239.22
Voltage feedback resistor	1404.08
Total occupied area	**4300**

IV. SYSTEM SIMULATION AND VALIDATION

After successfully performing DRC, LVS and extraction, the extracted view was simulated in nominal conditions (T = 300 K), to test the final operation of the system.

Figure 21 presents the testbench used. The models previously presented for the PV cell , and the battery are used in this simulation to achieve a more accurate indication of what would be the real operation of the system. Different setups were used to test the system for the different conditions that were considered in the design stage.

The first test that was carried out considers the PV cell under maximum light intensity and the battery deeply discharged. For this case, it is expected that S1 is on, with the PV cells

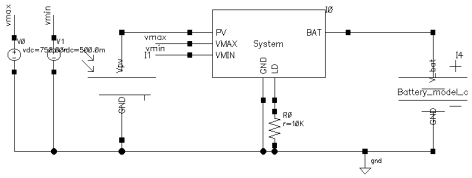

Fig. 21. System testbech.

charging the battery, and that S2 switch is off, since the battery does not have enough energy to feed the load. Figure 22 presents the relevant signals obtained for this first setup.

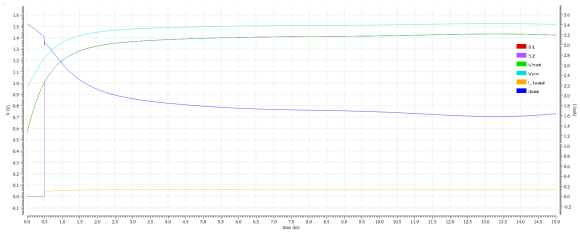

Fig. 22. Results for nominal simulation for the first setup test: initial SOC = -0.1 V, $R_{load} = 10\,k\Omega$ and Ipv = 4 mA.

In this scenario, the initial SOC is defined as -0.1 V, to ensure that the battery's initial voltage is below the EOD voltage, representing a more deeply discharged state. As expected, S2 is off in the initial stage. S1 is on, since V_{pv} is higher than V_{bat}. The initial charging current is higher, corresponding to the rapid voltage increase that takes place when the charging process is initiated, as previously described in Section 2, when the battery's charging process was analyzed. After this initial stage, the charging current stabilizes to approximately 1.7 mA. S2 is turned on exactly when the battery's voltage reaches 1 V, which happens after approximately 8 minutes. From this moment on, the system feeds the load with a constant current of 140 μ A, while the battery is continually charged by the PV cells.

The second test considers when there is no available light to power the PV cell, but the battery is half charged. The results for this scenario is presented in 23.

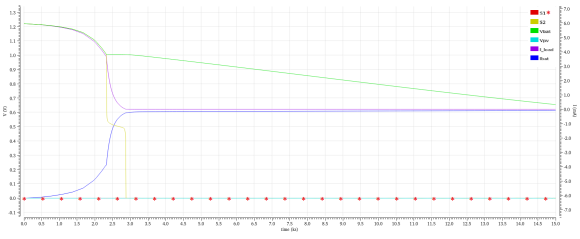

Fig. 23. Results for nominal simulation for the second setup test: initial SOC = 0.5 V, $R_{load} = 100\,\Omega$ and Ipv = 0.

For this case, an initial SOC of 0.5 V was defined, which corresponds to an initial V_{bat} of approximately 1.2 V. S1 is off since the PV cell do not generate any voltage. A load of 100 Ω was used to optimize simulation time while ensuring that the battery reaches the EOD voltage. In the initial stage, the battery is used to feed the load with a current of roughly 5.9 mA. Around 1.5 mA the battery is used to operate the system, which totals an output discharge current in the vicinity of -6.12 mA. The battery is capable of supplying this current up to around 25 minutes, after which the considered EOD voltage is achieved, and S2 is turned off.

A parametric analysis was carried out, with different I_{pv} values to oversee the system's behavior under different lightning conditions. The results obtained are presented in Figure 24.

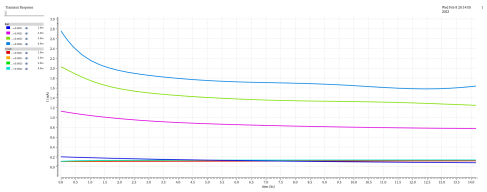

Fig. 24. I_{bat} and I_{load} currents under different lightning conditions.

As expected, the charging rate is proportional to the charging current, which in this case is the current made available by the PV cells. Table VIII presents a summary of some charging characteristics and how these vary with the input solar cells current.

TABLE VIII
CHARGING CHARACTERISTICS UNDER DIFFERENT LIGHTNING CONDITIONS

Ipv (A)	t (Vbat=Vn)	I (t=10000 s) (A)
1 m	3.9 h	158.9 μ
2 m	45.9 mn	825.8 μ
3 m	24.5 mn	1.33 m
4 m	16.6 mn	1.67 m

In the table above, the second column corresponds to the time that it takes for the battery to reach its nominal voltage of 1.2 V. The third column shows the stable charging current, using as reference the timestamp of 10000 s. These results are an indication that the system can still operate with reasonable performance, even when the PV cell is under a lower light intensity. Naturally, the higher the charging current, the faster the battery will charge to a desired voltage level.

Figures 25 a) and b) present the daily irradiance in Portugal, for a typical day in the months of December and July, respectively. Analyzing the data, one can see that the global incident irradiance available exceeds 200 W/m^2 during at least 8 hours on a winter day and for at least 11 hours on a summer day. Considering the V/I characteristic of the solar cells, presented in figure 25, the current corresponding to the situation in which the cells are under an irradiance of 200 W/m^2 are approximately 1 mA. Based on the obtained results, with 1 mA, the battery takes almost 4 hours to reach the nominal voltage, which can still be assured for a winter day. Depending of the application and of the final load value, this charging rate can be more or less desirable, but the current available is sufficient to charge the battery, even if under trickle charging conditions.

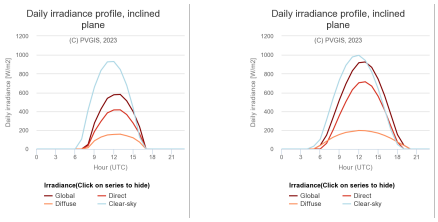

Fig. 25. Daily irradiance in Portugal: a) December; b) July.

A. Dispersion in the voltage references

As previously stated, the threshold voltages used to monitor the EOC and EOD levels of the battery are meant to be generated by an on-chip voltage reference circuit. Since the entire system is fed by the battery and the battery's voltage is variable over time, it is important to contemplate how these fluctuations can impact the reference voltages and the overall operation of the system. To account for this effect, a consideration had to be made on how these reference voltages vary with the bias voltage.

After a detailed researched on the already existent voltage reference circuits in 65 nm CMOS processes that more closely match the requirements for the reference values needed in the system, the circuits presented in [8] are considered. Examining the MOS circuit presented, it can be confirmed that the line regulation, defined by the expression in 15, is 3.8%, for an approximate reference voltage of 680 mV.

$$LR = \frac{\Delta V_{ref}}{V_{ref}} \times \frac{1}{\Delta V_{DD}} \times 100 \tag{15}$$

Considering the reference voltage dispersion that might occur, the bias voltage and the reference voltages can be described as

$$V_{DD} = V_{DD0} + \Delta V_{DD} \tag{16}$$

$$V_{ref} = V_{ref0} + \Delta V_{ref} \tag{17}$$

where for our system V_{DD} corresponds to V_{bat}. Substituting 15 in 17 and applying this variation to our reference values, the following relation can be obtained for the reference voltages:

$$V_{min} = 499.62m + 0.38m \times V_{bat}\ [V] \tag{18}$$

$$V_{max} = 749.43m + 0.38m \times V_{bat}\ [V] \tag{19}$$

When it comes to temperature, it is seen in simulation that for one of the chips, the temperature coefficient is 157 ppm/ºC. This is the value that will be considered in our system.

To simulate the system with these variable reference voltages, the two ideal sources present in figure 21 were replaced by voltage dependent voltage sources, following the variations described in 18 and 19, and the temperature coefficient of 157 ppm/ºC.

B. Corner analysis

A corner analysis was performed to test the system's operation for four different process variations related to the transistors' speed: FF (fast fast), FS (fast, slow), SF (slow, fast) and SS (slow, slow) and four different temperature values in the range of -40ºC to 120ºC, making a total of 16 corners situations. Figures 26 and 27 present the results obtained for the first test setup, which is the same that was used in the nominal system simulation.

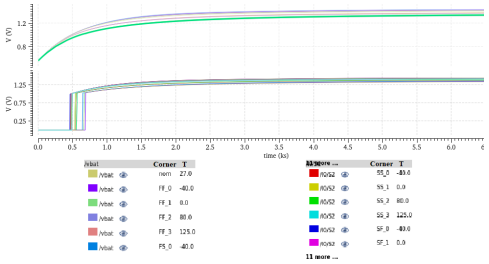

Fig. 26. V_{bat} and switch 2 control's signal variation with corners.

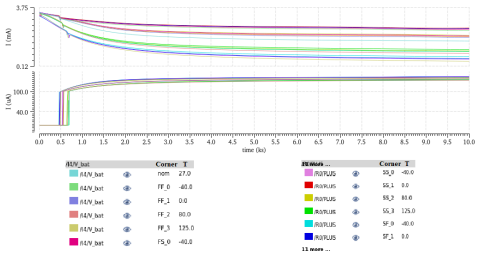

Fig. 27. I_{bat} and I_{load} variation with corners.

The variations considered also affect the PV cell model, altering its output voltage, which in turn affects the battery's charging rate. The deviations observed in these results are due essentially to the changes that these process variations introduce in the energy source model. Regardless of these changes, the behavior of the system is consistent with the working conditions and specified requirements, which is an indication of the validation of the system's correct operation under these different conditions.

C. System validation

To certify that the harvester is fit to operate as a battery charger for the 6VHR NiMH battery, an analysis should be made with the purpose of verifying if the developed system meets all the charging and safety recommendations supplied by the manufacturer. According to the technical information available in [9], three charging methods are contemplated for the 6VHR battery. These methods are summarized in table IX.

Considering the PV cells used in this work, the maximum charging current expected for the battery, is approximately 3 mA, which corresponds to the charging current indicated for accelerated charge. Despite the system not incorporating timing control, the overcharge protection implemented through voltage control certifies that the charging is interrupted when the battery reaches the EOC voltage, which typically happens

TABLE IX
CHARGING METHODS FOR THE 6VHR NIMH BATTERY EXTRACTED FROM THE DATASHEET

Charge Method	Current	Time	Control
Nominal	0.6 mA	14-16 h	Time
Accelerated	3 mA	4h	Time, voltage
Trickle	0.18 mA (max)	Unlimited	-

before the suggested charging time is reached. Additionally, even when the PV cell is under maximum light intensity, a percentage of the available current is used to operate the remaining blocks of the system, which means that the effective current used to charge the battery is obviously lower. Taking all this aspects into consideration, it is safe to admit that a safe charging process for the battery is ensured.

V. CONCLUSIONS

This work allowed the completion of a solar harvester battery charger system, in CMOS 65 nm process, capable of charging a 1.2 V battery NiMH from a nominal 1.2 V at 3.3 mA solar panel, while simultaneously supplying an end load.

Initially, a study was carried out on different equivalent circuit models that describe the electrical behavior of rechargeable NiMH batteries. An experimental procedure was developed to obtain an equivalent circuit model for the battery and the PV cells. An analysis was made on the proposed circuit solutions, based on the main specifications of the system, about the different blocks and circuits needed to accomplish it. These different blocks were then designed, and later fine-tuned, based on their behavior in the integrated system. A full layout of the system was developed, extracted and validated. Using the models developed for the PV cells and the battery, the full system was tested in simulation, for different lightning conditions, temperatures and process variations. The reference voltages' variations were also considered and analyzed, based on an existent BGR circuit to be implemented in the same chip. Finally, the system was validated taking into account the battery's charging/discharging requirements, and the simulation results that were obtained. The result is a fully integrated solar energy harvesting system, capable of safely charging a 1.2 V nominal NiMH battery, with overcharge and overdischarge protection.

ACKNOWLEDGMENTS

I would like to express my deepest appreciation and thanks to my supervisors professor Pedro Santos and professor João Vaz, for their invaluable guidance and relentless support throughout the duration of this work. A special thanks to *Instituto de Telecomunicações* and the *Wireless Circuits - Lx* research group for granting me this research opportunity and all the necessary equipment for the completion of this work.

REFERENCES

[1] M. Chen and G. Rincon-Mora, "Accurate Electrical Battery Model Capable of Predicting Runtime and I–V Performance," *IEEE Transactions on Energy Conversion*, vol. 21, no. 2, pp. 504–511, Jun. 2006. [Online]. Available: http://ieeexplore.ieee.org/document/1634598/

[2] A. Hentunen, T. Lehmuspelto, and J. Suomela, "Time-Domain Parameter Extraction Method for Thévenin-Equivalent Circuit Battery Models," *IEEE Transactions on Energy Conversion*, vol. 29, no. 3, pp. 558–566, Sep. 2014. [Online]. Available: http://ieeexplore.ieee.org/document/6811175/

[3] H. Rahimi-Eichi and M.-Y. Chow, "Adaptive parameter identification and State-of-Charge estimation of lithium-ion batteries," in *IECON 2012 - 38th Annual Conference on IEEE Industrial Electronics Society*. Montreal, QC, Canada: IEEE, Oct. 2012, pp. 4012–4017. [Online]. Available: http://ieeexplore.ieee.org/document/6389248/

[4] S. Abu-Sharkh and D. Doerffel, "Rapid test and non-linear model characterisation of solid-state lithium-ion batteries," *Journal of Power Sources*, vol. 130, no. 1-2, pp. 266–274, May 2004. [Online]. Available: https://linkinghub.elsevier.com/retrieve/pii/S0378775303011455

[5] W. Li, L. Liang, W. Liu, and X. Wu, "State of Charge Estimation of Lithium-Ion Batteries Using a Discrete-Time Nonlinear Observer," *IEEE Transactions on Industrial Electronics*, vol. 64, no. 11, pp. 8557–8565, Nov. 2017. [Online]. Available: http://ieeexplore.ieee.org/document/7926321/

[6] J. Cubas, S. Pindado, and C. de Manuel, "Explicit Expressions for Solar Panel Equivalent Circuit Parameters Based on Analytical Formulation and the Lambert W-Function," *Energies*, vol. 7, no. 7, pp. 4098–4115, Jun. 2014. [Online]. Available: http://www.mdpi.com/1996-1073/7/7/4098

[7] N. Khosropour, F. Krummenacher, and M. Kayal, "Fully integrated ultra-low power management system for micro-power solar energy harvesting applications," *Electronics Letters*, vol. 48, no. 6, p. 338, 2012. [Online]. Available: https://digital-library.theiet.org/content/journals/10.1049/el.2012.0315

[8] G. Traversi, F. D. Canio, L. Gaioni, M. Manghisoni, L. Ratti, and V. Re, "Design of bandgap reference circuits in a 65 nm CMOS technology for HL-LHC applications," *Journal of Instrumentation*, vol. 10, no. 02, pp. C02 004–C02 004, Feb. 2015. [Online]. Available: https://iopscience.iop.org/article/10.1088/1748-0221/10/02/C02004

[9] V. Microbattery, "Rechargeable button cells nimh - sales program and technical handbook." [Online]. Available: https://www.varta-ag.com/fileadmin/varta_microbattery/downloads/service/battery-documentation/nickel-metal-hydride/Sales-Literature-201810_HANDBOOK_Rechargeable_Button_Cells_NiMH_en.pdf